

Annual Review of Control, Robotics, and Autonomous Systems

Communication-Aware Robotics: Exploiting Motion for Communication

Arjun Muralidharan and Yasamin Mostofi

Department of Electrical and Computer Engineering, University of California, Santa Barbara, California 93106, USA; email: arjunm@ece.ucsb.edu, ymostofi@ece.ucsb.edu

Annu. Rev. Control Robot. Auton. Syst. 2021. 4:115–39

First published as a Review in Advance on January 11, 2021

The Annual Review of Control, Robotics, and Autonomous Systems is online at control.annualreviews.org

https://doi.org/10.1146/annurev-control-071420-

Copyright © 2021 by Annual Reviews. All rights reserved

ANNUAL CONNECT

www.annualreviews.ora

- Download figures
- · Navigate cited references
- Keyword search
- · Explore related articles
- Share via email or social media

Keywords

communication-aware path planning, exploiting mobility for connectivity, real channel environments, probabilistic channel prediction, co-optimization of motion and communication, first passage distance, minimum-energy operation, robotic routers, robotic beamformers

Abstract

In this review, we present a comprehensive perspective on communication-aware robotics, an area that considers realistic communication environments and aims to jointly optimize communication and navigation. The main focus of the article is theoretical characterization and understanding of performance guarantees. We begin by summarizing the best prediction an unmanned vehicle can have of the channel quality at unvisited locations. We then consider the case of a single robot, showing how it can mathematically characterize the statistics of its traveled distance until connectivity and further plan its path to reach a connected location with optimality guarantees, in real channel environments and with minimum energy consumption. We then move to the case of multiple robots, showing how they can utilize their motions to enable robust information flow. We consider two specific robotic network configurations—robotic beamformers and robotic routers—and mathematically characterize properties of the co-optimum motion—communication decisions.

1. INTRODUCTION

The past few decades have brought unprecedented growth in sensing, communication, computation, and actuation, driving a revolution in sensor networks and robotics. Teams of autonomous robots, each equipped with sensing and communication capabilities, can sense and interact with their environment and cooperatively work toward achieving a common goal. Such robotic networks are envisioned to play an increasingly important role in a wide range of tasks, including emergency response, surveillance, service provisioning, agriculture, data gathering, and extending cellular network coverage.

Wireless communication plays an integral role in robotic network operations because unmanned vehicles need to connect to other nodes or to a remote operator—for instance, to transfer sensing data and/or to receive control commands. Maintaining connectivity and ensuring a robust flow of information are thus fundamental problems in robotic networks. Since each robot's path directly affects its link quality, each unmanned vehicle needs to take the communication quality into account when path planning.

This area of research, where a group of unmanned vehicles explicitly take communication link qualities into account when path planning, is known as communication-aware robotics. In communication-aware robotics, each node explicitly assesses the impact of its motion decisions on its link quality and co-optimizes its communication, navigation, and sensing objectives. This results in interesting interplay among the optimum motion, communication, and sensing parameters, as these parameters are now coupled in the decision-making process. Considering the underlying energy constraints, in terms of both communication and navigation, further creates interesting interplay between the communication and motion decisions.

Figure 1 shows sample scenarios of networked robotic operations. Communication-aware robotics is the main topic of this review, with a special focus on utilizing the motion of the robots to enable or optimize connectivity and to co-design the underlying communication and navigation objectives.

1.1. The State of the Art

The idea of multirobot systems began in the 1980s [with, e.g., the seminal work of Fukuda & Nakagawa (1)], followed by much more extensive work in the following decades on a wide range of applications. Due to the already-complex nature of multirobot operations in terms of path planning, distributed decision-making, and sensing, earlier work in multirobot systems did not consider communication issues. In the past decade, however, the importance of jointly considering communication objectives, along with motion and sensing goals, has been recognized. For instance, the impact of communication has been considered in several networked robotic tasks, such as coverage control (2–4), field sensing (5, 6), search and surveillance (7–11), target tracking (12), flocking (13–15), consensus (16, 17), simultaneous localization and mapping (SLAM) (18, 19), task allocation and servicing (20–23), and robotic routing protocols (24, 25).

In more recent years, a new set of applications has also emerged where unmanned vehicles are used to extend the connectivity of cellular systems or indoor home/office router networks (see **Figure 1***c,d*). This has resulted in a broad range of recent work on using the mobility of robotic systems to enable and optimize communication. For instance, robot mobility can be exploited for point-to-point communication (26–32), relaying (33–41), beamforming (42–46), data gathering (47–54), and communication coverage (55, 56).

Historically, earlier work in communication-aware robotics utilized oversimplified models of connectivity, such as disk models or path loss-only models (7, 11, 34, 36, 48), due to the









Figure 1

Sample robotic operations (best viewed in color): (*a*) search and rescue, (*b*) mobile service provisioning, (*c*) extending coverage of cellular systems, and (*d*) optimizing the connectivity of home networks. Background images courtesy of the US Navy (panel *a*), Getty Images (panel *b*), and Pixabay (panels *c* and *d*).

already-complex nature of the underlying multirobot problem. Such models, however, cannot properly capture the spatial variations of wireless links in real environments (e.g., see the sample channel measurement shown in **Figure 2b**). Thus, control strategies built on such oversimplified models can experience significant performance degradation when implemented in practice. More recent work has utilized more realistic channel models. For instance, Mostofi and colleagues (57, 58) introduced a probabilistic channel prediction framework by considering the three major

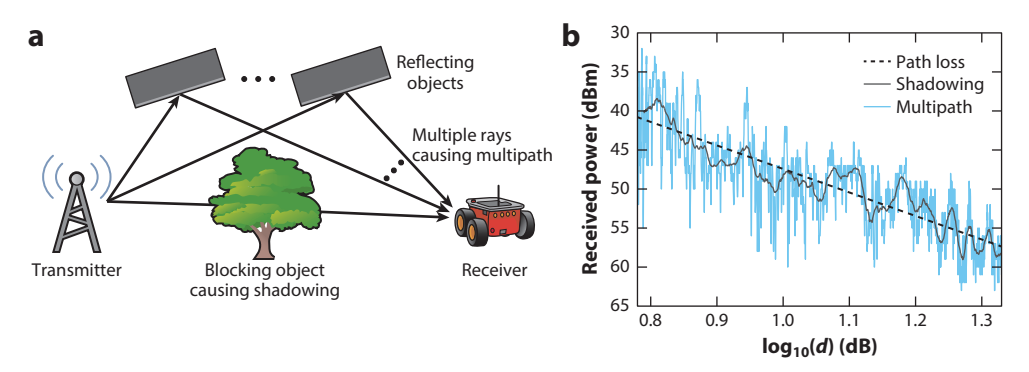


Figure 2

(a) A toy environment that illustrates the channel components. (b) A sample of received power along an indoor route together with its underlying dynamics: path loss, shadowing, and multipath. Figure adapted with permission from Reference 57.

Connected location:

a location $q_1 \in \mathbb{R}^2$ where the received channel power is greater than the minimum required channel power [i.e., $\Gamma(q_1) \ge \gamma_{th}$]

underlying dynamics of the channel, which allows the robots to estimate a probability density function (PDF) of the channel quality at unvisited locations, based on a small number of a priori or online channel samples. This probabilistic framework has since been utilized in numerous robotics works (4, 8, 12, 28, 31, 35, 38, 44, 45, 47, 50, 59–67) and has interesting implications for robotic path planning and networked robotic operations.

1.2. Review Outline

Our goal in this review is to present a comprehensive perspective on communication-aware robotics and the corresponding co-optimization of communication and navigation in realistic channel environments, with an emphasis on theoretical characterization and understanding performance guarantees.

In Section 2, we review a realistic channel model that utilizes the main three dynamics of wireless links: path loss, shadowing, and multipath. We then mathematically characterize the best prediction an unmanned vehicle can have of the channel quality at unvisited locations, based on a small number of online or a priori channel samples. As we shall see, the best prediction is a probabilistic estimate that builds a PDF for the channel at an unvisited location, using the three underlying dynamics mentioned above.

We then discuss the case of a single robot in Sections 3 and 4, with the goal of presenting a mathematical understanding of optimum communication-aware robotic decisions. Here, we see how an unmanned vehicle can mathematically characterize the statistics of its distance traveled until connectivity and further plan its path to reach a guaranteed connected location, with minimum energy consumption, and while achieving an asymptotic ϵ -suboptimal solution.

In Section 5, we move to the case of multiple robots utilizing their motions to enable robust information flow and connectivity. We consider two specific robotic network configurations: robotic beamformers and robotic routers. Our focus is on understanding and mathematically characterizing properties of the co-optimum motion—communication decisions and the interplay between the two. In Section 6, we then briefly mention other aspects of communication—aware robotics. Finally, we summarize the key findings and discuss potential future directions.

2. CHANNEL MODELING AND PREDICTION

Traditionally, ideal communication links or disk models have been heavily utilized in the robotics literature in order to spatially model a communication link at unvisited locations for the purpose of path planning. In a disk model, there is perfect connectivity within a certain radius of a transmitting node, with no connection outside of it. A disk model, however, is a poor representation of the link quality. Figure 2b, for instance, shows a real channel measurement (57); as can be seen, the link is far from ideal, and a disk model would be a poor representation of the link. In more recent years, it has been acknowledged that a better prediction of the link quality is needed for the purpose of robotic field operation, and that consequently a more multidisciplinary approach is needed that jointly considers both communication and navigation issues. Along this line, new methods have been developed, based on empirical channel models, that aim to probabilistically predict the channel power at unvisited locations based on a number of online or a priori channel samples in the area. In this section, we review this realistic probabilistic modeling of the spatial variations of a wireless channel and the subsequent prediction framework that allows the robots to probabilistically predict the channel at unvisited locations (57, 58). This probabilistic framework has been utilized by multiple robotics works in the last decade (4, 8, 12, 28, 31, 35, 38, 44, 45, 47, 50, 59-67).

2.1. Probabilistic Channel Modeling

In the communications literature, a wireless channel is well modeled as a random process with three main spatial dynamics: (a) a slowly varying (with respect to space) path loss component that accounts for decay in the channel power with distance; (b) a quickly varying shadowing component (also called large-scale fading) that accounts for the attenuation effects of buildings, trees, and other large obstructing structures; and (c) an even more quickly varying multipath component (also called small-scale fading) that accounts for scattering and reflection (68). **Figure 2**b shows a sample of received channel power along an indoor route together with its constituent dynamics.

Let $\Gamma(q_1)$ denote the received channel power (in decibels) at location $q_1 \subset \mathbb{R}^2$ due to a transmitting station located at $q_b \in \mathbb{R}^2$. Then,

$$\Gamma(q_1) = \gamma_{\text{PL}}(q_1) + \Gamma_{\text{SH}}(q_1) + \Gamma_{\text{MP}}(q_1), \qquad 1.$$

where $\gamma_{PL}(q_1) = K_{dB} - 10n_{PL} \log_{10} \|q_1 - q_b\|$ is the path loss component, with n_{PL} denoting the path loss coefficient. $\Gamma_{SH}(q_1)$ is the shadowing component and is best modeled as a zero-mean Gaussian random process with an exponentially decaying correlation function: $\mathbf{E}[\Gamma_{SH}(q_1)\Gamma_{SH}(q_2)] = \sigma_{SH}^2 e^{-\|q_1 - q_2\|/\beta_{SH}}$, with σ_{SH}^2 representing the shadowing power and β_{SH} denoting the decorrelation distance (68). Finally, $\Gamma_{MP}(q_1)$ is the multipath component and is also best modeled as a random process, with several distributions (such as Nakagami, Rician, and lognormal) found to be good fits for its distribution (68, 69).

2.2. Probabilistic Channel Prediction

We next see how an unmanned vehicle can use the previous empirical channel modeling to probabilistically predict the channel power at unvisited locations (i.e., predict the corresponding PDFs) based on online or a priori channel samples in the area (57, 58).

Let $\Gamma_q = [\Gamma_{q_1}, \dots, \Gamma_{q_m}]^T$ denote the vector of m collected channel measurements at locations $q = [q_1, \dots, q_m]^T$ in the workspace of interest. This small number of measurements can be collected by the robot before the operation. Alternatively, they can be collected by other robots in past operations and stored in the cloud. The robot can also use the channel measurements it collects during the operation to predict the channel at unvisited locations in an online manner.

The following theorem (57) shows how the robot can estimate the channel at unvisited locations based on a small number of prior samples.

Theorem 1. A Gaussian random vector $\Gamma(r) = [\Gamma(r_1), \dots, \Gamma(r_k)]^T \sim \mathcal{N}(\overline{\Gamma}(r), \Sigma(r))$ can best characterize the channel power (in decibels) at unvisited locations $r = [r_1 \dots r_k]^T$, with the mean and covariance matrix given by

$$\overline{\Gamma}(r) = G_r \hat{\vartheta} + \Xi_{r,q} \left(\Xi_q + \hat{\sigma}_{MP}^2 I_m \right)^{-1} \left(\Gamma_q - G_q \hat{\vartheta} \right),$$
 2.

$$\Sigma(r) = \Xi_r + \hat{\sigma}_{MP}^2 I_k - \Xi_{r,q} \left(\Xi_q + \hat{\sigma}_{MP}^2 I_m \right)^{-1} \Xi_{r,q}^T,$$
3.

respectively. Here, $G_r = [\mathbf{1}_k - L_r]$ and $G_q = [\mathbf{1}_m - L_q]$ (where $\mathbf{1}_m$ and $\mathbf{1}_k$ represent the m-dimensional and k-dimensional vector of all ones, respectively); I_m and I_k represent the m-dimensional and k-dimensional identity matrices, respectively; $L_q = \begin{bmatrix} 10\log_{10}(\|q_1-q_b\|) \dots 10\log_{10}(\|q_m-q_b\|) \end{bmatrix}^{\mathrm{T}}$; and $L_r = \begin{bmatrix} 10\log_{10}(\|r_1-q_b\|) \dots 10\log_{10}(\|r_k-q_b\|) \end{bmatrix}^{\mathrm{T}}$ (where q_b is the position of the remote station). Furthermore, Ξ_q , Ξ_r , and $\Xi_{r,q}$ denote matrices with entries $\left[\Xi_q\right]_{i_1,i_2} = \hat{\sigma}_{\mathrm{SH}}^2 e^{-\|q_{i_1}-q_{i_2}\|/\hat{\beta}_{\mathrm{SH}}}$, $\left[\Xi_r\right]_{j_1,j_2} = \hat{\sigma}_{\mathrm{SH}}^2 e^{-\|r_{j_1}-r_{j_2}\|/\hat{\beta}_{\mathrm{SH}}}$, and $\left[\Xi_{r,q}\right]_{j_1,j_1} = \hat{\sigma}_{\mathrm{SH}}^2 e^{-\|r_{j_1}-q_{i_1}\|/\hat{\beta}_{\mathrm{SH}}}$, respectively, where $i_1,i_2\in\{1,\ldots,m\}$ and $j_1,j_2\in\{1,\ldots,k\}$. Moreover, $\vartheta=[K_{\mathrm{dB}}-n_{\mathrm{PL}}]^{\mathrm{T}}$, β_{SH} , σ_{SH}^2 , and σ_{MP}^2 denote the path loss parameters, the

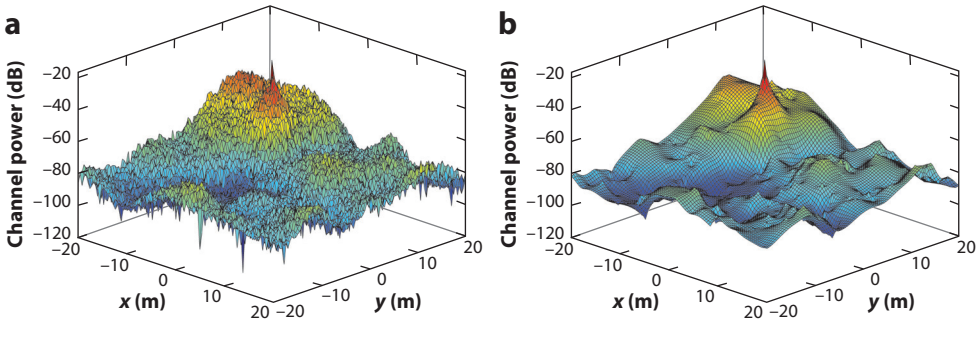


Figure 3

(a) The mean of the estimated channel power based on a small number of randomly distributed prior measurements (5%) of (b) the true channel map in a 2D workspace.

decorrelation distance of shadowing, the power of shadowing (in decibels), and the power of multipath (in decibels), respectively. The ^ symbol denotes the estimate of the corresponding parameter.

The underlying channel parameters can be estimated from a few a priori measurements as well (for more details, see 57). Using this framework, the robot can then predict a PDF for the channel at unvisited locations of the workspace for the purposes of path planning. **Figure 3** shows a sample 2D channel and its predicted mean from Theorem 1 using 5% prior channel samples in the space. Note that the predicted variance at each unvisited location can then serve as the corresponding uncertainty in channel learning.

We next start with one robot and see how it can mathematically characterize and optimize its connectivity before moving to a network of unmanned vehicles.

3. DISTANCE TRAVELED UNTIL CONNECTIVITY

Consider the scenario where a robot is seeking to establish a connection with a remote node as it moves along a predefined path, as shown in **Figure 4**. One important factor that the robot may need to assess is its distance until connectivity (i.e., how much longer it needs to travel before it

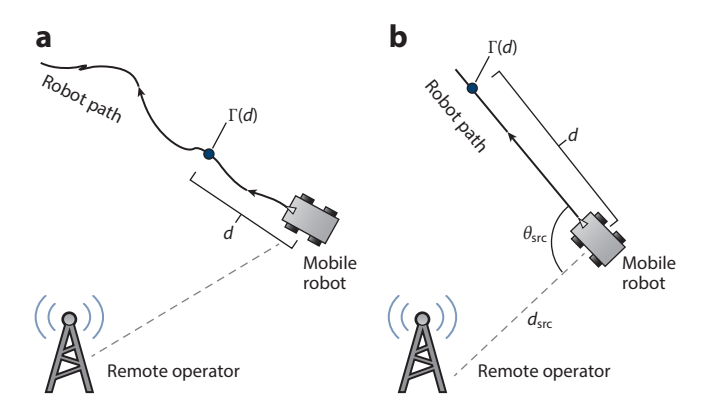


Figure 4

What is the distance traveled by the robot before it finds a connected location along (*a*) a general path and (*b*) a straight path? Figure adapted with permission from Reference 28.

becomes connected), as this distance can play a key role in its field decision-making. We next characterize how the robot can mathematically characterize the PDF of its distance until connectivity (28) using the probabilistic channel model of Section 2.

Establishing connectivity requires that a certain quality of service (such as a minimum bit error rate) be satisfied, which in turn translates to a minimum required channel power, which we shall denote by γ_{th} . A location q is thus said to be connected if $\Gamma(q) \ge \gamma_{th}$.

With a slight abuse of notation, for the remainder of this section, let $\Gamma(d) = \gamma_{\rm PL}(d) + \Gamma_{\rm SH}(d) +$ $\Gamma_{\rm MP}(d)$ denote the channel power at a distance d along the given path. We are then interested in characterizing the distance traveled by the robot until it finds a connected location. Muralidharan & Mostofi (32) referred to this distance as the first passage distance (FPD), drawing a parallel with the concept of first passage time. We next see how to mathematically characterize the PDF of the ϵ -upcrossing FPD, which is the FPD given that the robot is initially disconnected. More specifically, the random variable $\mathcal{D}_{\Gamma_0}^{\epsilon} = \inf_{d>0} \{d: \Gamma(d) \geq \gamma_{\text{th}} | \Gamma(0) < \gamma_{\text{th}} - \epsilon \}$ denotes the ϵ -upcrossing FPD, where $\Gamma(0)$ is a random variable upper bounded by $\gamma_{th} - \epsilon^2$ Consider the complementary cumulative distribution function (CCDF) of $\mathcal{D}_{\Gamma_0}^{\epsilon}: \Pr(\mathcal{D}_{\Gamma_0}^{\epsilon} > d) = \Pr(\Gamma(b) < 1)$ $\gamma_{\rm th}$, $\forall b < d \mid \Gamma(0) < \gamma_{\rm th} - \epsilon$), which is what the robot is interested in evaluating. A direct naive computation of this would involve a high-dimensional prohibitive integration over the probabilistic Gaussian channel model of Section 2. In other words, assuming we discretize the path into N steps and the domain of $\Gamma(d)$ into M parts, this would have a computational complexity of $O(NM^N)$, which quickly becomes infeasible for even moderate values of N and M. We next see how the robot can mathematically evaluate its FPD in a way that is both theoretically meaningful and computationally efficient—that is, $O(N^2)$ when multipath is negligible and $O(NM \log(M))$ otherwise.

We start by considering the statistics of the FPD for a straight path, and then characterize the FPD for a more general space of paths.

3.1. First Passage Distance for a Straight Path

Consider a robot starting from an initial distance of $d_{\rm src}$ from the remote station and traveling along a straight path in the direction specified by $\theta_{\rm src}$, as shown in **Figure 4**. The path loss component $\gamma_{\rm PL}(d)$ is then expressed as $\gamma_{\rm PL}(d) = K_{\rm dB} - 5n_{\rm PL}\log_{10}(d_{\rm src}^2 + d^2 - 2d_{\rm src}d\cos\theta_{\rm src})$.

We first consider the case where multipath is negligible, followed by a more general analysis with multipath included.

3.1.1. The case of negligible multipath: stochastic differential analysis. Characterization of FPD while ignoring multipath effects is directly applicable to cases where multipath is negligible due to a low number of scatterers or when we want to find a small area of good connectivity as opposed to a single well-connected location. Moreover, this analysis provides further insight into the general FPD characterization.

For negligible multipath, we are then interested in when $\Gamma(d) = \gamma_{PL}(d) + \Gamma_{SH}(d)$ is greater than γ_{th} . As summarized in the following lemma (28), $\Gamma_{SH}(d)$ and subsequently $\Gamma(d)$ can be shown to be Gauss–Markov processes (see the sidebar titled Gauss–Markov Processes).

First passage distance (FPD): the distance traveled by a robot along a path until a connection is established

¹First passage time is the time until a random process first hits a threshold (70). It has been extensively used in diverse fields, including Brownian motion modeling, neuronal firing characterization, and stock market analysis.

²We require that $\epsilon > 0$ since the mathematical tools used are not well defined for $\epsilon = 0$. However, ϵ can be considered arbitrarily small.

GAUSS-MARKOV PROCESSES

Gaussian Process

A stochastic process $\{X(t): t \in \mathcal{T}\}$, where \mathcal{T} is an index set, is a Gaussian process if any finite number of samples have a joint Gaussian distribution; that is, $(X(t_1), X(t_2), \dots, X(t_k))$ is a Gaussian random vector for all $t_1, \dots, t_k \in \mathcal{T}$ and for any k (71). A Gaussian process is completely specified by its mean function $m_X(t) = \mathbb{E}[X(t)]$ and its covariance function $\Sigma_X(t_1, t_2) = \mathbb{E}\{[X(t_1) - m_X(t_1)][X(t_2) - m_X(t_2)]\}$. We use the notation $X \sim \mathcal{GP}(m_X, \Sigma_X)$ to denote the underlying process.

Markov Process

A process X(t) is a Markov process if $\Pr(X(t_n) \le x_n | X(t_{n-1}), \dots, X(t_1)) = \Pr(X(t_n) \le x_n | X(t_{n-1}))$, for all n and for all $t_n \ge t_{n-1} \ge \dots \ge t_1$, where $\Pr(\cdot)$ denotes the probability of the argument (72).

Gauss-Markov Process

A stochastic process is a Gauss–Markov process if it satisfies the requirements of both a Gaussian process and a Markov process (73).

Lemma 1. The channel shadowing power $\Gamma_{SH}(d)$ and subsequently the channel power $\Gamma(d)$ are Gauss–Markov processes with characterizations $\mathcal{GP}(0, \Sigma_{SH})$ and $\mathcal{GP}(\gamma_{PL}, \Sigma_{SH})$, respectively, where $\Sigma_{SH}(b,d) = \sigma_{SH}^2 e^{-(d-b)/\beta_{SH}}$.

In fact, $\Gamma_{SH} \sim \mathcal{GP}(0, \Sigma_{SH})$ is the famous Ornstein–Uhlenbeck process, one of the most well-studied Gauss–Markov processes (74).

Using the Gauss–Markov literature (75), one can show that the transition PDF $f(\gamma, d|\eta, b)$ characterizing the distribution of $\Gamma(d)$ given $\Gamma(b) = \eta$ satisfies the partial differential equation known as the Fokker–Planck equation (28), as follows:

$$\frac{\partial}{\partial d} f(\gamma, d|\eta, b) = -\frac{\partial}{\partial \gamma} \left[A_{\rm FP}(\gamma, d) f(\gamma, d|\eta, b) \right] + \frac{1}{2} \frac{\partial^2}{\partial \gamma^2} \left[B_{\rm FP} f(\gamma, d|\eta, b) \right], \tag{4}$$

with the associated initial condition of $f(\gamma, b|\eta, b) = \delta(\gamma - \eta)$, where $A_{\rm FP}(\gamma, d) = \gamma'_{\rm PL}(d) - (\gamma - \gamma_{\rm PL}(d))/\beta_{\rm SH}$, $B_{\rm FP} = (2\sigma_{\rm SH}^2)/\beta_{\rm SH}$, $\gamma_{\rm PL}(d)$ is the path loss component, and $\gamma'_{\rm PL}(d)$ is its derivative.

The channel power $\Gamma(d)$ can also be represented as a stochastic differential equation,

$$d\Gamma(d) = A_{\rm FP}(\Gamma, d)dd + \sqrt{B_{\rm FP}}d\overline{W}(d),$$
 5.

where $\overline{W}(d)$ represents the Wiener process, and $A_{\rm FP}(\gamma,d)$ and $B_{\rm FP}$ are as defined above.

Remark 1. $A_{\text{FP}}(\gamma, d)$ and B_{FP} are known as the drift and diffusion components, respectively. More specifically, in an increment Δd , we can think of the channel power spatially evolving with a deterministic rate of $A_{\text{FP}}(\gamma, d)$, while a zero-mean random Gaussian term with the variance of $B\Delta d$ is superposed on it.

The following result builds on the Fokker–Planck equation and provides a recursive integral equation to find the PDF of the ϵ -upcrossing FPD (28).

Theorem 2. Let $g_u^{(\epsilon)}[d]$ denote the PDF of the ϵ -upcrossing FPD. Then, $g_u^{(\epsilon)}[d]$ satisfies the following nonsingular second-kind Volterra integral equation:

$$g_u^{(\epsilon)}[d] = -2\Psi_u^{(\epsilon)}[d] + 2\int_0^d g_u^{(\epsilon)}[b]\Psi[d|\gamma_{\text{th}}, b]db,$$
 6.

where

$$\begin{split} \Psi[d|\eta,b] &= \bigg\{ -\frac{1}{2} \frac{\mathrm{d}\gamma_{\mathrm{PL}}(d)}{\mathrm{d}d} - \frac{\gamma_{\mathrm{th}} - \gamma_{\mathrm{PL}}(d)}{2\beta_{\mathrm{SH}}} \frac{1 + e^{-2(d-b)/\beta_{\mathrm{SH}}}}{1 - e^{-2(d-b)/\beta_{\mathrm{SH}}}} \\ &+ \frac{\eta - \gamma_{\mathrm{PL}}(b)}{\beta_{\mathrm{SH}}} \frac{e^{-(d-b)/\beta_{\mathrm{SH}}}}{1 - e^{-2(d-b)/\beta_{\mathrm{SH}}}} \bigg\} f(\gamma_{\mathrm{th}}, d|\eta, b), \Psi_u^{(\epsilon)}[d] \\ &= \frac{1}{2\mathrm{Pr}(\Gamma(0) < \gamma_{\mathrm{th}} - \epsilon)} \bigg\{ \frac{-2\sigma_{\mathrm{SH}}^2}{\beta_{\mathrm{SH}}} e^{-d/\beta_{\mathrm{SH}}} f(\gamma_{\mathrm{th}} - \epsilon, 0) f[\gamma_{\mathrm{th}}, d|\gamma_{\mathrm{th}} - \epsilon, 0] \\ &+ \frac{1}{2} f(\gamma_{\mathrm{th}}, d) (1 + \mathrm{Erf}[\gamma_{\epsilon}(d)]) \bigg(-\frac{\mathrm{d}\gamma_{\mathrm{PL}}(d)}{\mathrm{d}d} - \frac{1}{\beta_{\mathrm{SH}}} [\gamma_{\mathrm{th}} - \gamma_{\mathrm{PL}}(d)] \bigg) \bigg\}, \end{split}$$

with $\operatorname{Erf}(z) = \frac{2}{\sqrt{\pi}} \int_0^z e^{-t^2} dt$ representing the error function, and

$$\Upsilon_{\epsilon}(d) = \frac{\gamma_{\rm th} - \epsilon - \gamma_{\rm PL}(0) - e^{-d/\beta_{\rm SH}} \left(\gamma_{\rm th} - \gamma_{\rm PL}(d)\right)}{\sqrt{2\sigma_{\rm SH}^2 \left(1 - e^{-2d/\beta_{\rm SH}}\right)}}.$$

This enables the robot to mathematically characterize the PDF of its distance until connectivity. Furthermore, the recursive integral of Theorem 2 serves as the basis for an efficient iterative algorithm (using Simpson's rule) to compute the PDF of the FPD in $O(N^2)$ (for details, see 75).

3.1.2. Including multipath effects: a recursive characterization. In this section, we consider the more general channel model of $\Gamma(d) = \gamma_{\rm PL}(d) + \Gamma_{\rm SH}(d) + \Gamma_{\rm MP}(d)$. The results of Section 3.1.1 are no longer applicable since the overall channel power $\Gamma(d)$ is not a Gauss–Markov process once we include the multipath component in our analysis. However, the shadowing power $\Gamma_{\rm SH}(d)$ is still a Markov process, and we can use this to obtain a methodology to compute the PDF of the FPD recursively. Let us assume that the robot measures the channel along the straight path in discrete steps of size Δd . We further assume that the multipath component is uncorrelated at two points separated by Δd , which is a reasonable assumption since the multipath component typically decorrelates quickly (57). We then index the channel power based on the steps taken, that is, let $\Gamma_k = \Gamma(k\Delta d)$ and $\Gamma_{\rm SH,k} = \Gamma_{\rm SH}(k\Delta d)$.

We are then interested in the characterization of the FPD $\mathcal{K} = \min_{1,2,...} \{k : \Gamma_k \geq \gamma_{th}, \Gamma_0 < \gamma_{th}\}$. This can be expressed in terms of its CCDF as

$$\Pr(\mathcal{K} = k) = \Pr(\mathcal{K} > k - 1) - \Pr(\mathcal{K} > k).$$
 7.

Note that this CCDF probability can be expressed as

$$\Pr\left(\mathcal{K} > k\right) = \Pr\left(\Gamma_1, \dots, \Gamma_k < \gamma_{\text{th}} \middle| \Gamma_0 < \gamma_{\text{th}}\right),$$
8.

where

$$\Omega_k(\gamma_{\mathrm{SH},k}) = \int_{\gamma_{\mathrm{MP},k} = -\infty}^{\gamma_{\mathrm{th}} - \gamma_{\mathrm{PL}}(d_k) - \gamma_{\mathrm{SH},k}} \int \dots \int_{S_{k-1}} p\left(\gamma_{\mathrm{SH},0}, \gamma_{\mathrm{MP},0}, \dots, \gamma_{\mathrm{SH},k}, \gamma_{\mathrm{MP},k}\right)$$

$$\times d\gamma_{SH,0}d\gamma_{MP,0}\dots d\gamma_{SH,k-1}d\gamma_{MP,k-1}d\gamma_{MP,k}, \qquad 9.$$

with $S_{k-1} = \bigcap_{i=0}^{k-1} \left\{ \gamma_{\text{SH},i}, \gamma_{\text{MP},i} : \gamma_{\text{PL}}(d_i) + \gamma_{\text{SH},i} + \gamma_{\text{MP},i} < \gamma_{\text{th}} \right\}$ and $p\left(\gamma_{\text{SH},0}, \gamma_{\text{MP},0}, \dots, \gamma_{\text{SH},k}, \gamma_{\text{MP},k}\right)$ representing the joint probability density of $\Gamma_{\text{SH},0}, \Gamma_{\text{MP},0}, \dots, \Gamma_{\text{SH},k}$, and $\Gamma_{\text{MP},k}$.

We can compute the functions $\Omega_k(\gamma_{SH,k})$ recursively as shown in the following lemma (28).

Lemma 2. The functions Ω_k of Equation 9, for k = 1, ..., N, can be computed by the recursion

$$\Omega_{k+1}(\gamma_{\text{SH},k+1}) = F_{\text{MP}}(\gamma_{\text{th}} - \gamma_{\text{PL}}(d_{k+1}) - \gamma_{\text{SH},k+1}) \frac{1}{\varrho} \int_{u=-\infty}^{\infty} \varphi\left(\frac{\gamma_{\text{SH},k+1} - u}{\sigma_{\text{SH}}\sqrt{1-\varrho}}\right) \Omega_k\left(\frac{u}{\varrho}\right) du, \qquad 10.$$

initialized with $\Omega_0(\gamma_{SH,0}) = F_{MP}(\gamma_{th} - \gamma_{PL}(0) - \gamma_{SH,0}) \varphi\left(\frac{\gamma_{SH,0}}{\sigma_{SH}}\right)$, where $F_{MP}(\cdot)$ is the cumulative distribution function of the multipath random variable Γ_{MP} and $\varphi(\cdot)$ is the standard Gaussian density function.

We can then use Lemma 2 to efficiently calculate the PDF of the FPD using Equations 7 and 8.

3.2. First Passage Distance for a General Path

The results of the previous section were for a straight path and utilized the fact that the shadowing power $\Gamma_{SH}(d)$ is a Gauss–Markov process on a straight path. The channel shadowing power along a general nonstraight path, however, may not be a Gauss–Markov process. Still, we can characterize a large set of paths for which the shadowing power is approximately Markovian and use the results of the previous section to characterize the FPD.

Consider a point at a distance d along a general path, as shown in Figure 4a. The shadowing power at this point and at the point a step behind (for a step size of Δd) are given by $\Gamma_{SH}(d)$ and $\Gamma_{SH}(d-\Delta d)$, respectively. The FPD characterization of Section 3.1 followed from the Markovian nature of the shadowing power—that is, $p(\gamma_{SH}(d)|\gamma_{SH}(d-\Delta d), \{\gamma_{SH}(d-b), \forall b > 0\})$ Δd) = $p(\gamma_{SH}(d)|\gamma_{SH}(d-\Delta d))$. Thus, a path is approximately Markovian if at every point on the path, these two distributions are close. We use the Kullback-Leibler (KL) divergence (see the sidebar titled Kullback-Leibler Divergence) between the distributions as a measure of how close they are. The smaller the KL divergence is, the closer the path is to Markovian, and the more applicable the characterization of the FPD of Section 3.1 will be. However, mathematically characterizing the KL divergence between these two distributions can be intractable. Instead, we consider the pairwise KL divergences between $p(\gamma_{SH}(d)|\gamma_{SH}(d-\Delta d),\gamma_{SH}(d-b))$ and $p(\gamma_{SH}(d)|\gamma_{SH}(d-\Delta d))$ for all $b>\Delta d$ and for all d. If these pairwise KL divergences are small enough, we declare the path to be approximately Markovian. The KL divergence between the distributions of $\Gamma_{SH}(d)|\Gamma_{SH}(d-\Delta d)$, $\Gamma_{SH}(d-b)$ and $\Gamma_{SH}(d)|\Gamma_{SH}(d-\Delta d)$ for a $b>\Delta d$ is a chisquared random variable (77). We then formally define an approximately Markovian path as follows (see 28).

KULLBACK-LEIBLER DIVERGENCE

KL divergence is a measure of the distance between two distributions (76). The KL divergence between two distributions p(x) and $\tilde{p}(x)$ is defined as

$$KL = \int p(x) \log_e \frac{p(x)}{\tilde{p}(x)} dx.$$

We utilize the KL divergence as a measure of how close to Markovian the channel shadowing power along a general path is.

Definition 1 (approximately Markovian path). Let $m_{\text{KL}}(d,b)$ and $\sigma_{\text{KL}}(d,b)$ denote the mean and standard deviation of the KL divergence between $p(\gamma_{\text{SH}}(d)|\gamma_{\text{SH}}(d-\Delta d), \gamma_{\text{SH}}(d-b))$ and $p(\gamma_{\text{SH}}(d)|\gamma_{\text{SH}}(d-\Delta d))$ for a given $b > \Delta d$. A path is approximately Markovian for parameters ϵ_m and ϵ_σ if $m_{\text{KL}}(d,b) \le \epsilon_m$ and $\sigma_{\text{KL}}(d,b) \le \epsilon_\sigma$ for all $b > \Delta d$ and for all d.

We can determine whether a path is approximately Markovian, for parameters ϵ_m and ϵ_σ , based purely on properties of the path (e.g., its curvature) and the underlying channel parameters (e.g., decorrelation distance). The intuition here is that if the curvature of the path is small enough, and if the path does not loop around, then the path can be considered approximately Markovian. The following theorem (28) formalizes this intuition and precisely characterizes sufficient conditions for an approximately Markovian path.

Theorem 3 (approximately Markovian path). Let r(d) = (x(d), y(d)) be a path parameterized by its arc length. The path is approximately Markovian for given maximum tolerable KL divergence parameters ϵ_m and ϵ_σ if it satisfies two conditions: First, $||r(d) - r(d-b)|| > d_{\rm th}$ for $b > \frac{1}{\kappa} \sin^{-1}(\kappa d_{\rm th})$ and for all d, and second, curvature $\kappa(d) < \kappa_{\rm th}$ for all d, where $d_{\rm th} = \frac{\beta_{\rm SH}}{2} \log_{\epsilon} \left(\varrho^2 + \frac{1-\varrho^2}{\epsilon_d} \right)$ and $\kappa_{\rm th}$ is obtained by solving the following optimization problem:

maximize
$$\kappa$$
 subject to $\max_{\phi:0<\phi\leq\psi_{\mathrm{cons}(\kappa)}}\psi_{\mathrm{opt}}(\kappa,\phi)\leq\epsilon_d,$ 11.
$$\kappa<1/d_{\mathrm{th}},$$

where

$$\psi_{\text{opt}}(\kappa,\phi) = \frac{\left(e^{-\frac{2}{\kappa\beta_{\text{SH}}}\sin\left(\frac{\phi+\Delta\phi}{2}\right)} - \varrho e^{-\frac{2}{\kappa\beta_{\text{SH}}}\sin\left(\frac{\phi}{2}\right)}\right)^{2}}{\left(1 - e^{-\frac{4}{\kappa\beta_{\text{SH}}}\sin\left(\frac{\phi}{2}\right)}\right)(1 - \varrho^{2})},$$

$$\psi_{\mathrm{cons}}(\kappa) = 2\sin^{-1}\left(\frac{\kappa d_{\mathrm{th}}}{2}\right) - \Delta\phi, \quad \Delta\phi = 2\sin^{-1}\left(\frac{\kappa\Delta d}{2}\right), \quad \varrho = e^{-\Delta d/\beta_{\mathrm{SH}}}, \quad \mathrm{and} \quad \epsilon_d = \min\{1 - e^{-2\epsilon_m}, \sqrt{2}\epsilon_\sigma\}.$$

Note that several general paths satisfy the conditions of Theorem 3, as shown by Muralidharan & Mostofi (28). For instance, **Figure 5a** shows an Archimedean spiral path, which can be confirmed to be approximately Markovian. **Figure 5b** further shows the cumulative distribution function of the ϵ -upcrossing FPD for this path using Lemma 2. We can see that the theoretical derivations are a good match to the true statistics obtained via Monte Carlo simulations. The underlying channel was generated with parameters obtained from real channel measurements in downtown San Francisco (78).

The results of this section show how an unmanned vehicle can theoretically characterize the statistics of its distance traveled until connectivity in a mathematical framework that is also computationally very efficient.

4. PATH PLANNING TO ESTABLISH CONNECTIVITY

In this section, we consider the case where the robot can also plan its path such that it minimizes the expected traveled distance until it finds a guaranteed connected location to a remote station (30, 31). The robot, operating in a realistic channel environment experiencing path loss, shadowing,

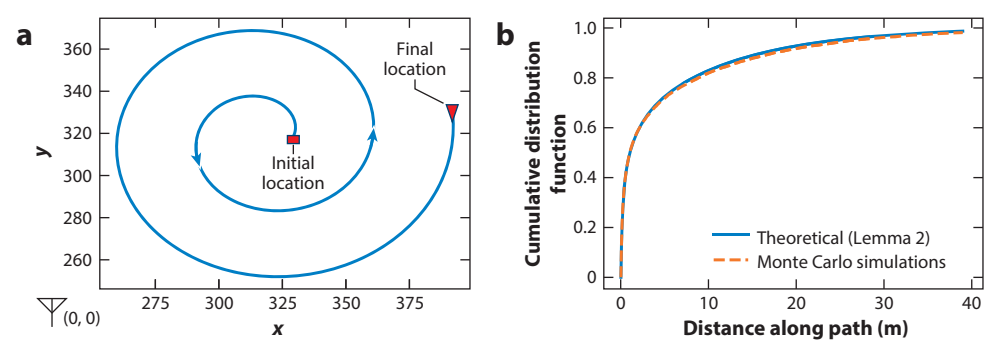


Figure 5

(a) An Archimedean spiral as the path of a robot. (b) The cumulative distribution function of the upcrossing first passage distance when including multipath using Lemma 2. Figure adapted with permission from Reference 28.

and multipath fading, has an estimate of the connectivity across space using the channel prediction framework of Section 2. The robot can then plan its path and exploit this channel prediction such that it minimizes the expected traveled distance until it becomes connected (see **Figure 6a**). As we shall see, this problem can be solved with asymptotic optimality guarantees in a graph-theoretic setting (31).

Let us discretize the workspace of the robot into cells to form a grid graph $\mathcal{G}=(\mathcal{V},\mathcal{E})$, with each cell serving as a node in the graph. Each node $v\in\mathcal{V}$ is associated with a probability of connectivity $p_v\in[0,1]$, and each edge $(u,v)\in\mathcal{E}$ is associated with a length $l_{u,v}>0$ representing the distance between two nodes u and v in the workspace. A cell is connected if there exists a location in the cell that is connected. For instance, consider a cell/node v that consists of positions $r=[r_1,\ldots,r_k]^T$. The probability of connectivity of cell v is then given by $p_v=1-\Pr(\Gamma(r_i)<\gamma_{th},\forall i\leq k)$, where $\Gamma(r)=[\Gamma(r_1)\ldots\Gamma(r_k)]^T\sim\mathcal{N}\left(\overline{\Gamma}(r),\Sigma(r)\right)$ is a Gaussian random vector obtained from the channel prediction framework of Section 2, and γ_{th} is the minimum required channel

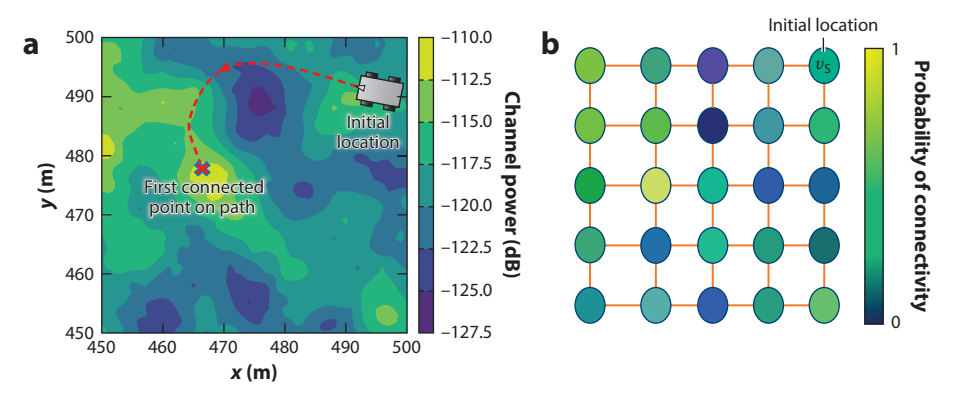


Figure 6

A robot plans its path such that it minimizes the expected distance until it becomes connected to a remote station, in a realistic channel environment that experiences path loss, shadowing, and multipath fading.

(a) The workspace of the robot with the background representing the mean of the predicted channel quality.

(b) The graph-theoretic representation of the workspace, where every node is associated with a probability of connectivity derived from the predicted channel quality. Panel a adapted with permission from Reference 30.

power for connectivity. For the mathematical analysis of this section, we assume that the probability of connectivity at a node is independent of the connectivity at any other node in the workspace.

The objective is to then generate a path, starting from a node $v_s \in \mathcal{V}$, that minimizes the expected traveled distance until connectivity. Note that the robot may traverse only part of the generated path, as its planning is based on a probabilistic channel characterization, and it may become connected at any node along the path. For the expected traveled distance until connectivity to be well defined for a path, the probability of failure after traversing the entire path must be zero, implying that the final node must be a node where $p_v = 1$. We call such a node a terminal node and define $T = \{v \in \mathcal{V} : p_v = 1\}$. For instance, the remote station can serve as a terminal node. The expected cost of a path $\mathcal{P} = (v_1, v_2, \dots, v_m = v_t)$ can then be expressed as $C(\mathcal{P}) = \sum_{e \in \mathcal{E}(\mathcal{P})} [\prod_{v \in \mathcal{V}(\mathcal{P}_e)} (1 - p_v)] l_e$, where $\mathcal{E}(\mathcal{P})$ denotes the set of edges belonging to the path \mathcal{P} , and $\mathcal{V}(\mathcal{P}_e)$ denotes the set of vertices encountered along \mathcal{P} until the edge $e \in \mathcal{E}(\mathcal{P})$. Note that the robot estimates the probability of connectivities $(p_v s)$ using the probabilistic prediction framework of Section 2. The optimization problem of interest, which we refer to as the Min-Exp-Dist-Path problem, can then be posed as (31)

Min-Exp-Dist-Path problem:

problem: the optimization problem to find the path that minimizes the expected traveled distance until connectivity

$$\underset{\mathcal{P}}{\text{minimize}} \quad C(\mathcal{P}) = \sum_{e \in \mathcal{E}(\mathcal{P})} \left[\prod_{v \in \mathcal{V}(\mathcal{P}_e)} (1 - p_v) \right] l_e$$
12.

subject to \mathcal{P} is a path of \mathcal{G} such that $\mathcal{P}[1] = v_s, \mathcal{P}[\text{end}] \in T$.

Theorem 4. The Min-Exp-Dist-Path problem of Equation 12 is an NP-hard problem.

The proof is based on showing that the decision version of the problem is NP complete, using a reduction to a rooted version of the NP-complete Hamiltonian path problem (31).

We next see how an ϵ -suboptimal solution to Equation 12 can be achieved by posing this problem in a game-theoretic setting (see the sidebar titled Game Theory Primer). Note that, in what follows, the robot is using game theory solely to design its own path and as such can make all the decisions locally.

GAME THEORY PRIMER

A game $\{\mathcal{V}', \{A_v\}, \{\mathcal{J}_v\}\}\$ consists of the following components: (a) the players (agents) of the game, \mathcal{V}' ; (b) the action set of player v, A_v ; and (c) the local cost function of player $v, \mathcal{J}_v : A \to \mathbb{R}$, where $A = \prod_{u \in \mathcal{V}'} A_u$.

Nash Equilibrium

An action profile μ^{NE} is said to be a pure Nash equilibrium if $\mathcal{J}_v(\mu^{\text{NE}}) \leq \mathcal{J}_v(\mu_v, \mu_{-v}^{\text{NE}})$, $\forall \mu_v \in A_v, \forall v \in \mathcal{V}'$, where μ_{-v} denotes the action profile of all players except v (79).

Potential Game

 $\{\mathcal{V}', \{A_v\}, \{\mathcal{J}_v\}\}\$ is a potential game over action space $A_S \subset A$ if there exists a function $\Phi: A_S \to \mathbb{R}$ such that $\mathcal{J}_v(\mu'_v, \mu_{-v}) - \mathcal{J}_v(\mu_v, \mu_{-v}) = \Phi(\mu'_v, \mu_{-v}) - \Phi(\mu_v, \mu_{-v})$, for all $\mu = (\mu_v, \mu_{-v}) \in A_S$, $v \in \mathcal{V}'$, and μ'_v such that $(\mu'_v, \mu_{-v}) \in A_S$, where μ_{-v} denotes the action profile of all players except v (31, 80).

Upstream node:

a node u in the directed graph $SG(\mu)$ when another node v lies on the directed path from u to the corresponding sink; the node u is then said to be upstream of v

4.1. Game-Theoretic Communication-Aware Path Planner

Consider a game $\{\mathcal{V}', \{A_v\}, \{\mathcal{J}_v\}\}$ where the set of nonterminal nodes $\mathcal{V}' = \mathcal{V}/\mathcal{T}$ of the previously defined graph are the players of the game, and the action set $A_v = \{u \in \mathcal{V} : (u, v) \in \mathcal{E}\}$ is the set of neighbors of node v. Let $\mu_v \in A_v$ be the action of player/node v, and let μ be the joint action profile.

We first describe the path produced from a node v and its expected distance until connectivity in terms of the action profile μ . An action profile μ induces a directed graph, $\mathcal{SG}(\mu)$, on \mathcal{G} , which has directed edges from v to μ_v . A node u is said to be upstream of v in $\mathcal{SG}(\mu)$ if v lies on the directed path from u to the corresponding sink. We denote the set of upstream nodes of v as $U_v(\mu_{-v})$ and let $v \in U_v(\mu_{-v})$ by definition. Let $\mathcal{P}(\mu,v)$ be the directed path from node v on $\mathcal{SG}(\mu)$, and let $C_v(\mu) = C(\mathcal{P}(\mu,v))$ denote the expected cost from node v when following the path $\mathcal{P}(\mu,v)$. Let $A_{\rm ASG}$ denote the set of action profiles such that the expected cost $C_v(\mu) < \infty$ for all $v \in \mathcal{V}$. This will happen only if the path $\mathcal{P}(\mu,v)$ ends at a terminal node for all v. This corresponds to $\mathcal{SG}(\mu)$ being a directed acyclic graph with terminal nodes as sinks. Then $\mu \in A_{\rm ASG}$ implies that the action of player v belongs to the constrained action set $A_v^c(\mu_{-v})$ [i.e., $\mu_v \in A_v^c(\mu_{-v})$], where $A_v^c(\mu_{-v}) = \{u \in \mathcal{V} : (v,u) \in \mathcal{E}, u \notin U_v(\mu_{-v}), C_u(\mu) < \infty\}$ is the set of actions that result in a finite expected cost from v.

Next, consider local cost functions \mathcal{J}_v of the form

$$\mathcal{J}_{v}(\mu) = \sum_{u \in U_{v}(\mu)} \varsigma_{u} C_{u}(\mu),$$
13.

where $U_v(\mu)$ is the set of upstream nodes of v, and $\varsigma_u > 0$ are constants such that $\varsigma_{v_s} = 1$ and $\varsigma_v = \epsilon'$, for all $v \neq v_s$, where $\epsilon' > 0$ is a small constant. These local cost functions then result in a potential game over $A_{\rm ASG}$, as summarized in the next lemma (for the proof, see 31).

Lemma 3. The game $\{\mathcal{V}', \{A_v\}, \{\mathcal{J}_v\}\}\$, with local cost functions as defined in Equation 13, is a potential game over A_{ASG} with a potential function

$$\Phi(\mu) = \sum_{v \in \mathcal{V}'} \varsigma_v C_v(\mu) = C_{v_s}(\mu) + \epsilon' \sum_{v \neq v_s} C_v(\mu).$$
 14.

4.1.1. Asymptotically ϵ -suboptimal path planner. We shall next see how to asymptotically obtain the global minimizer of $\Phi(\mu)$ and thereby find an ϵ -suboptimal solution to the Min-Exp-Dist-Path problem of Equation 12, by utilizing a learning process known as log-linear learning (31, 81).

Consider a potential game over the following complete graph. The complete graph $\mathcal{G}_{\text{comp}}$ is formed from \mathcal{G} by adding an edge between all nodes that do not share an edge. The length of an added edge (u, v) is set to be the shortest distance between u and v. Then, the log-linear process operating on this potential game with constrained action sets $A_v^c(\mu_{-v}(k))$ asymptotically reaches an ϵ -suboptimal solution to the Min-Exp-Dist-Path problem, as formally summarized below (31).

Theorem 5. Consider the Min-Exp-Dist-Path problem of Equation 12. Consider loglinear learning on a potential game over the complete graph \mathcal{G}_{comp} with local cost functions as defined in Equation 13, and $\epsilon' = \epsilon / (|\mathcal{V}'|D)$, where D is the diameter of the graph. Then, as the temperature τ associated with log-linear learning goes to zero (i.e., $\tau \to 0$), the process asymptotically provides an ϵ -suboptimal solution to the Min-Exp-Dist-Path problem.

4.1.2. Fast non-myopic path planner. Log-linear learning provides an ϵ -suboptimal solution to the Min-Exp-Dist-Path problem asymptotically. However, in certain scenarios, finding a suboptimal but fast solution may be more important.

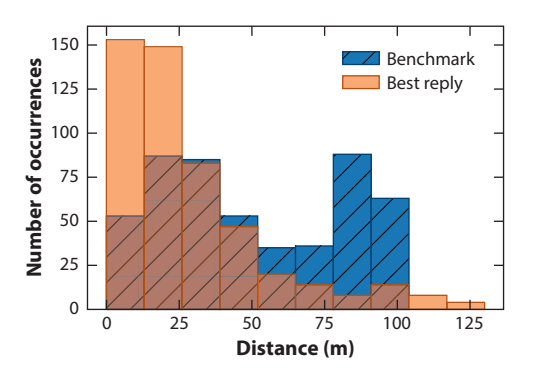


Figure 7

Histogram of the traveled distance for the best-reply approach of Section 4.1.2 and a benchmark (where the robot moves straight toward the remote station) over 500 channel realizations. Figure adapted with permission from Reference 31.

The best-reply process (79) operating on the potential game of Lemma 3 with constrained action sets $A_v^\epsilon(\mu_{-v}(k))$ converges to a pure Nash equilibrium, which is also a directionally local minimum of $\Phi(\mu) = C_{v_s}(\mu) + \epsilon' \sum_{v \neq v_s} C_v(\mu)$ (for more details, see 31). The best-reply process converges quickly to a directionally local minimum [e.g., after at most $|\mathcal{V}'|$ iterations (31)] and is thus an efficient path planner.

Figure 7 shows the histogram of the distance traveled until connectivity for a robot for the best-reply path planner as well as a heuristic approach of moving straight toward the remote station, which we use as a benchmark. The histogram is over 500 channel realizations, where the underlying channel is generated using real channel parameters from downtown San Francisco (78) and the traveled distance is calculated based on the true channel quality. We can see that the distance associated with the best-reply planner is much smaller than that associated with the benchmark. Log-linear learning performs the same as or better than the best-reply approach at a larger computation cost.

Overall, this section has shown how an unmanned vehicle can optimize its path to get to a connected location, in realistic channel environments and with minimum energy consumption. As we saw, by using probabilistic channel prediction and a game theory–inspired path planning approach, it was possible to find an asymptotic ϵ -suboptimal global solution to this problem as well as fast solutions that can achieve a Nash equilibrium.

5. MULTIROBOT NETWORK CONNECTIVITY

In Sections 3 and 4, we considered the scenario of a single robot utilizing its motion to enable and optimize its connectivity with a remote station under energy constraints. In this section, we consider the case where multiple robots exploit their motion to cooperatively enable and optimize connectivity in realistic communication environments. Depending on the task at hand, a team of unmanned vehicles may need to form different network configurations to enable the needed connectivity and information flow. For instance, a particular task may need the nodes to keep a fully connected network throughout the operation, while another task may require a less-connected network or may allow the nodes to become momentarily disconnected from the team. While the nodes can in principle utilize their mobility to realize any given network configuration with a desired level of connectivity, here we focus on two particular network configurations, robotic beamformers and robotic routers, which can enable connectivity in otherwise poorly connected areas.

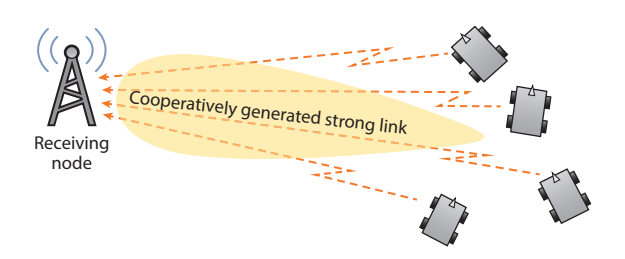


Figure 8

Distributed robotic transmit beamforming, in which multiple robots cooperatively generate a strong communication link to a remote station by optimizing their locations. Figure adapted with permission from Reference 45.

5.1. Cooperative Robotic Beamforming

Consider the scenario shown in **Figure 8**, where unmanned vehicles in a poorly connected area want to exploit their mobility to cooperatively generate a strong link to a remote station, which we refer to as cooperative robotic beamforming.

In traditional transmit beamforming, a number of colocated antennas align their transmission phases such that the wireless signals constructively merge at the remote station, providing dramatic gains in the received signal power (82). In distributed beamforming, this is extended to several fixed nodes distributed across space, which emulates a virtual antenna array (83, 84). In effect, transmit beamforming allows nodes to cooperatively generate a strong link, with dramatic gains in signal-to-noise ratio. The existing literature (83, 84) also describes how to effectively deal with timing and phase synchronization issues to produce the constructive interference required for beamforming in a distributed setting. Karanam et al. (85) further showed how to do beamforming with only signal magnitude, which can be useful if phase synchronization is not possible.

We can then extend the same concept to a team of unmanned vehicles and further utilize the vehicles' mobility to move to better locations for distributed transmit beamforming. Consider the scenario shown in **Figure 8**, where unmanned vehicles need to establish connectivity to a remote node, but the link quality for establishing individual communication is not strong enough in the area. The unmanned vehicles can utilize their mobility to move to locations that are best for forming a virtual distributed antenna array for transmit beamforming. Such robotic beamforming networks have been the subject of several studies (42–46). We next pose the underlying communication and motion co-optimization problem in real channel environments and discuss how an ϵ -suboptimal solution can be achieved (45).

Consider a case where N_r robots are in a poorly connected area, with r_i denoting the position of robot i. As discussed in Sections 3 and 4, successfully connecting to the remote station requires satisfying a minimum received channel power, γ_{th} . The received channel power (in the linear domain) at the remote station, after cooperative transmit beamforming by the N_r robots, is given by $(\sum_{i=1}^{N_r} \alpha(r_i)\rho_i)^2$, where $\alpha(r_i) = 10^{\Gamma(r_i)/20}$ is the channel amplitude when transmitting from location r_i , and $\rho_i \in [0,1]$ is the fraction of the maximum allowable transmit power used by robot i. Note that $\Gamma(r_i)$ denotes the received channel power in decibels when transmitting from location r_i . Let r and ρ denote the vector of the robot locations and the transmission coefficients, respectively. The connectivity constraint on the overall beamformed signal can then be expressed as $\sum_{i=1}^{N_r} \alpha(r_i)\rho_i \geq \sqrt{\gamma_{\text{th},\text{lin}}}$, where $\gamma_{\text{th},\text{lin}} = 10^{\gamma_{\text{th}}/10}$ is the minimum required channel power in the linear domain. The robots can utilize the channel prediction framework of Section 2 to obtain a conservative estimate of the channel amplitude $\tilde{\alpha}(r_i)$ at an unvisited location r_i , such that

Robotic beamforming:

the cooperative generation of a strong link by unmanned vehicles in an otherwise poorly connected environment $20 \log_{10} \tilde{\alpha}(r_i) = \overline{\Gamma}(r_i) - \zeta \sigma(r_i)$ for some constant $\zeta \ge 0$, where $\mathcal{N}(\overline{\Gamma}(r_i), \sigma(r_i)^2)$ is the predicted channel power distribution (in decibels) when transmitting from r_i , obtained from Theorem 1.

The optimization problem of how to successfully connect to the remote station while minimizing the total energy consumption can then be expressed as follows (45), where the unmanned vehicles must co-optimize their motion variables (r) and communication transmit power (ρ):

$$\begin{aligned} & \underset{r_{i},\rho_{i}}{\text{minimize}} & K_{\text{M}} \sum_{i=1}^{N_{r}} \|r_{i} - r_{i}^{0}\| + \frac{n_{\text{bits}}}{\mathcal{R}(r,\rho)} P_{0} \sum_{i=1}^{N_{r}} \rho_{i}^{2} \\ & \text{subject to} & \sum_{i} \tilde{\alpha}(r_{i}) \rho_{i} \geq \sqrt{\gamma_{\text{th,lin}}}, \\ & 0 \leq \rho_{i} \leq 1, \ i = 1, \dots, N_{r}, \end{aligned}$$

where $K_{\rm M} \sum_{i=1}^{N_r} \|r_i - r_i^0\|$ is the total motion energy consumed to move to final locations r_i 's from initial locations r_i^0 's, with $K_{\rm M}$ denoting the motion energy coefficient, and $\frac{n_{\rm bits}}{\mathcal{R}(r,\rho)} P_0 \sum_{i=1}^{N_r} \rho_i^2$ is the communication energy needed to transmit $n_{\rm bits}$ of information at rate

$$\mathcal{R}(r,\rho) = \pi_1 W \log_2 \left(1 + \pi_2 P_0 \frac{\left(\sum_{i=1}^{N_r} \tilde{\alpha}(r_i) \rho_i\right)^2}{N_0} \right),$$

where W, N_0 , and P_0 represent a robot's bandwidth, noise power, and maximum transmit power, respectively, and π_1 and π_2 are constants that depend on the communication scheme.

Theorem 6. The ϵ -suboptimal solution (final locations r and transmission coefficients ρ) to the optimization problem of Equation 15 can be found by solving $O(N_r/\epsilon)$ multiplechoice knapsack problems.

Reference 45 provides the proof and more details for the multiple choice knapsack problems. Theorem 6 shows that the robotic beamforming problem can be solved in realistic communication environments with performance guarantees. It also provides simulation results on robotic beamforming in realistic communication environments using Equation 15, which illustrates the benefits of motion and communication co-optimization.

5.2. Robotic Router Formation

An interesting problem in communication-aware robotics is that of robotic router formation for optimizing connectivity, which has been a topic of considerable interest (33–35, 39, 86, 87). Consider the case where two remote field nodes need to communicate but are too far from each other. A number of unmanned vehicles can act as mobile routers and move to positions optimal for routing the information between the remote nodes, as illustrated in **Figure 9**. In earlier work, graph-theoretic approaches were utilized to optimize the connectivity of a mobile relay network, without considering realistic communication channels or end-to-end performance metrics, while more recent work has considered co-optimization of communication and motion parameters in realistic channel environments. We start by discussing graph-theoretic approaches to solve this problem, and then consider the true cost of communication and co-optimizing motion and communication parameters.

5.2.1. A graph-theoretic approach to robotic routers. The Fiedler eigenvalue is a measure of how connected a graph is and can be used as a measure of the connectivity within a robotic

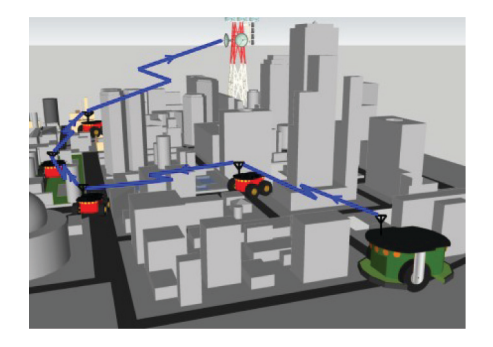


Figure 9

Robotic router formation, in which multiple robots need to move to the best positions for them to act as relays between two remote nodes that are too far apart to directly establish connectivity.

network (39, 86) or between two remote nodes (33). Thus, one possible solution to the robotic router position optimization problem is to have the unmanned vehicles form a graph that has a high Fiedler eigenvalue. Consider the state-dependent graph $\mathcal{G} = (\mathcal{V}, \mathcal{E})$, denoting the network of mobile robots, where the set of vertices $\mathcal{V} = \{1, \ldots, N_r\}$ is the set of N_r nodes, with the first and last nodes indicating the fixed remote nodes and the rest denoting the $N_r - 2$ robots. Let $r = [r_1, \ldots, r_{N_r}]^T$ denote the locations of the nodes. Stump et al. (33) modeled an edge between robots i and j in the graph as a distance-dependent weight $w(r_i, r_j) = f_{\text{conn}} \left(\| r_i - r_j \| \right)$ that uses a disk model, as follows: f_{conn} is 1 when the distance between robots i and j is less than a threshold and rapidly drops to 0 as the distance increases beyond the threshold (39). The weighted graph Laplacian matrix $\mathcal{L}_{\mathcal{G}}(r)$ is given by the entries

$$[\mathcal{L}_{\mathcal{G}}(r)]_{ij} = \begin{cases} -w(r_i, r_j), & \text{if } i \neq j, \\ \sum_{i \neq k} w(r_i, r_k), & \text{if } i = j. \end{cases}$$

We then have the following optimization problem to maximize the Fiedler eigenvalue of the robotic network (33):

$$\underset{r_{i}}{\text{maximize}} \quad \lambda_{2} \left(\mathcal{L}_{\mathcal{G}}(r) \right), \tag{16}$$

where λ_2 ($L_G(r)$) denotes the second-smallest eigenvalue of the Laplacian matrix (also known as the Fiedler value). Equation 16 can be solved using semidefinite programming (39) or via a decentralized algorithm using supergradient (86).

In this Fiedler value formulation, however, realistic channel models are not taken into account, and an oversimplified disk model is assumed. Furthermore, the true performance of a robotic router can be best characterized by how accurately it relays the transmitted bits between the two remote nodes. The next section poses a motion and communication co-optimization problem that takes these considerations into account.

5.2.2. Robotic router formation in realistic channel environments. Using the probabilistic channel prediction framework of Theorem 1, one can best model the channel power between the (i-1)th and ith robots, $\Gamma(r_{i-1}, r_i)$, as a Gaussian random variable with mean $\overline{\Gamma}(r_{i-1}, r_i)$ and standard deviation $\sigma(r_{i-1}, r_i)$. We can then pose the following optimization problem to maximize the probability of correct bit reception between the end nodes, for an M_s -QAM (quadrature amplitude

modulation) communication scheme (35):

maximize
$$\mathbb{E}\left\{\prod_{i=2}^{N_r} \left(1 - 0.2 \exp\left\{-\frac{1.5P_0}{(M_s - 1)N_0} 10^{\frac{\Gamma(r_{i-1}, r_i)}{10}}\right\}\right)\right\}$$
 subject to $r_i \in \mathcal{W}, i = 2, \dots, N_r - 1,$

where N_r is the total number of nodes, with the first and last nodes indicating the fixed remote nodes and $N_r - 2$ robots in between. Then, r_i is the location of the *i*th robot, $W \subseteq \mathbb{R}^2$ is the workspace of the robots, P_0 is the transmit power, N_0 is the noise power, and $\Gamma(r_{i-1}, r_i)$ is the random variable denoting the estimate of the channel between the (i-1)th and *i*th nodes.

This optimization problem can be well approximated as follows (for details, see 35):

maximize
$$\sum_{i=2}^{N_r} \ln \left(1 - 0.2 \left(1 + \frac{1.5P_0}{(M_s - 1)N_0} \xi(r_{i-1}, r_i) 10^{\frac{\overline{\Gamma}(r_{i-1}, r_i)}{10}} \right)^{-\iota(r_{i-1}, r_i)} \right),$$
 18.

where $\iota(r_{i-1}, r_i) = (\exp\{(a\sigma(r_{i-1}, r_i))^2\} - 1)^{-1}$ and $\xi(r_{i-1}, r_i) = \exp\{1.5(a\sigma(r_{i-1}, r_i))^2\} - \exp\{0.5(a\sigma(r_{i-1}, r_i))^2\}$, with $a = \ln 10/10$.

This formulation allows for mathematical analysis, as summarized next.

Theorem 7. If $\sigma(r_{i-1}, r_i) < \frac{1}{a} \sqrt{\ln(n_{\text{PL}} + 1)}$,

$$\overline{\Gamma}(r_{i-1}, r_i) \ge 10 \log_{10} \left(\frac{n_{\text{PL}} + 1}{n_{\text{PL}}} \frac{(M_s - 1)N_0}{1.5P_0} \left(\iota(r_{i-1}, r_i) \xi(r_{i-1}, r_i) - \frac{\xi(r_{i-1}, r_i)}{n_{\text{PL}}} \right)^{-1} \right),$$

and the shadowing correlation is negligible, then the optimization problem of Equation 18 is concave for a convex workspace.

Reference 35 provides the proof. Theorem 7 characterizes conditions on the underlying channel parameters under which the overall maximization problem can become concave. Intuitively, the stated conditions are sufficient bounds on the uncertainty, which results from not knowing the true value of the channel, in order to make the problem concave.

Moreover, if the concavity condition holds, then the optimum solution has the following properties (see 35).

Theorem 8. Assume that the concavity condition of Theorem 7 holds. Then the optimal solution of Equation 18 satisfies three properties: (a) If $K_{\text{dB},i-i,i} > K_{\text{dB},j-1,j}$ and $\sigma(r_{i-1},r_i) = \sigma(r_{j-1},r_j)$, then $d_{i-1,j}^*$ is greater than $d_{j-1,j}^*$, where $d_{i-1,j}^*$ is the optimal distance between robots i-1 and i; (b) if

$$\begin{split} K_{\mathrm{dB},i-i,i} &= K_{\mathrm{dB},j-1,j}, \\ \overline{\Gamma}(r_{i-1},r_i) &\geq 10 \log_{10} \left(\frac{(M_s-1)N_0 \left(\exp\{1.5 \exp\{(a\sigma(r_{i-1},r_i))^2\} - 0.5\} - 1 \right)}{1.5P_0 \xi(r_{i-1},r_i)} \right), \\ \overline{\Gamma}(r_{j-1},r_j) &\geq 10 \log_{10} \left(\frac{(M_s-1)N_0 \left(\exp\{1.5 \exp\{(a\sigma(r_{j-1},r_j))^2\} - 0.5\} - 1 \right)}{1.5P_0 \xi(r_{j-1},r_j)} \right), \end{split}$$

and $\sigma(r_{i-1},r_i) > \sigma(r_{j-1},r_j)$, then $d^*_{i-1,i}$ is less than $d^*_{j-1,j}$; and (c) if $K_{\mathrm{dB},i-i,i} = K_{\mathrm{dB},j-1,j}$ and $\sigma(r_{i-1},r_i) = \sigma(r_{j-1},r_j)$, then $d^*_{i-1,i}$ is equal to $d^*_{j-1,j}$.

Theorem 8 methodically compares the length of two route chains as a function of the experienced underlying channel parameters. Intuitively, it shows that as the predicted mean of the channel becomes smaller (indicating a lower channel quality) or there is more uncertainty in channel

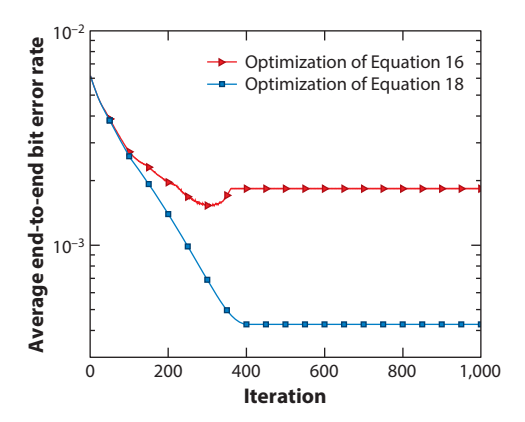


Figure 10

Robotic router optimization, comparing the graph-theoretic approach (Equation 16) with a channel-aware approach (Equation 18) in a realistic communication environment. Figure adapted with permission from Reference 35.

prediction (higher predicted channel variance), two consecutive robots should get closer to each other in the corresponding chain. Such mathematical characterizations can be valuable in designing robotic routers in realistic environments.

Figure 10 shows the performance of the optimization problem of Equation 18 as well as the graph-theoretic approach of Equation 16 in a realistic communication environment. We can see that incorporating realistic channel modeling and estimation has a significant impact on the performance. Yan & Mostofi (35) provided more details on the experimental results.

6. OTHER CONSIDERATIONS IN COMMUNICATION-AWARE ROBOTICS

Several other considerations are important in communication-aware robotics:

- Co-optimization of communication and motion: Co-optimization of communication and motion decisions results in interesting interplay among communication and motion parameters, such as waypoints, motion speed, transmission rate, and transmission power. Yan & Mostofi (65) jointly co-optimized the motion speed and transmission rate for a robot traveling along a predefined path, while Ali et al. (66) jointly designed the path/speed and the transmission rate/power along the path, using an optimal control framework.
- Co-optimization of communication and sensing: Explicitly considering sensing objectives and co-optimizing them with motion and communication has also been considered. For instance, Stachura & Frew (5) designed the path of an information-gathering aerial vehicle by jointly optimizing its sensing and communication. In a paper by Kemna et al. (6), teams of autonomous underwater vehicles planned their paths to collect informative samples while also optimizing information exchange. Ghaffarkhah & Mostofi (8, 12) explicitly co-optimized the sensing and communication objectives for networked robotic target tracking and surveillance.
- Distributed task servicing: In References 20–23, the robots decided how to efficiently allocate and service tasks among themselves, in a distributed fashion, while being aware of communication considerations. For example, in Reference 22, the robots executed tasks while maintaining desirable communication rates among themselves, and in Reference 21, the

- robots maintained connectivity while carrying out their tasks using underutilized robots as relays.
- Data gathering and muling: In References 48 and 54, robotic data mules planned their trajectories to gather data from stationary sensing nodes, assuming a disk model of connectivity. In Reference 51, an unmanned aircraft ferried data between two stationary nodes on a periodic trajectory and adaptively allocated the bandwidth along its trajectory to optimize the amount of transferred data.
- Search and surveillance: The area of multiple robots searching an area while maintaining a connected network to effectively cooperate has also been of interest. Bethke et al. (10) and Beard & McLain (11) maintained connectivity throughout the mission, while Hollinger & Singh (7) maintained only periodic connectivity. Ghaffarkhah & Mostofi (8) considered realistic channel environments and planned search trajectories for optimizing the detection while co-optimizing for communication with the remote station.

SUMMARY POINTS

- Instead of using oversimplified disk models, robots can use realistic channel models that
 consider the three major dynamics of path loss, shadowing, and multipath and probabilistically predict the channel at unvisited locations for the purpose of path planning.
 Theoretical results on different aspects of motion and communication co-optimization
 have built on this probabilistic framework.
- 2. An initially disconnected unmanned vehicle traveling along a predefined path can mathematically characterize the statistics of its traveled distance until connectivity (first passage distance), drawing from the literature on Gauss–Markov processes. It can further optimize its path to reach a guaranteed connected location with minimum energy consumption. For the latter, the robot can achieve an asymptotic ε-suboptimal solution to this optimization problem using a game-theoretic framework.
- The use of robotic beamformers and robotic routers, among other techniques, can allow
 multiple robots to optimize their locations or paths in order to cooperatively enable and
 optimize connectivity or flow of information.

FUTURE ISSUES

- The current state of the art in robotic channel prediction is the probabilistic channel modeling described in this review. Future work may find other ways to achieve a better channel prediction or to reduce the variance of the predicted model.
- A team of unmanned vehicles can in principle form any network formation that achieves any prescribed level of connectivity and information flow. However, more work is needed in this area to formally solve this problem, in terms of co-optimal motion and communication decisions.
- 3. Explicitly considering sensing goals in networked robotic operations is another line of future work. For instance, there is room for a more fundamental understanding of the co-optimal sensing, communication, and motion decisions in such networks. Devising algorithms that are independent of the specifics of a particular networked sensing operation can also be very beneficial.

4. Different aspects of communication-aware robotics have been considered and solved in different mathematical frameworks. A unifying approach to this area could be very useful and is a possible future direction.

DISCLOSURE STATEMENT

The authors are not aware of any affiliations, memberships, funding, or financial holdings that might be perceived as affecting the objectivity of this review.

ACKNOWLEDGMENTS

This work was supported in part by National Science Foundation Robust Intelligence award 1619376 and award 2008449.

LITERATURE CITED

- Fukuda T, Nakagawa S. 1987. A dynamically reconfigurable robotic system (concept of a system and optimal configurations). In *IECON'87: Industrial Applications of Robotics and Machine Vision*, pp. 588–95. Bellingham, WA: Soc. Photo-Opt. Instrum. Eng.
- Kantaros Y, Zavlanos MM. 2016. Distributed communication-aware coverage control by mobile sensor networks. Automatica 63:209–20
- Daniel K, Rohde S, Goddemeier N, Wietfeld C. 2010. A communication aware steering strategy avoiding self-separation of flying robot swarms. In 2010 5th IEEE International Conference on Intelligent Systems, pp. 254–59. Piscataway, NJ: IEEE
- Ghaffarkhah A, Mostofi Y. 2014. Dynamic networked coverage of time-varying environments in the presence of fading communication channels. ACM Trans. Sensor Netw. 10:45
- Stachura M, Frew E. 2017. Communication-aware information-gathering experiments with an unmanned aircraft system. J. Field Robot. 34:736–56
- Kemna S, Caron DA, Sukhatme GS. 2016. Adaptive informative sampling with autonomous underwater vehicles: acoustic versus surface communications. In OCEANS 2016 MTS/IEEE Monterey. Piscataway, NJ: IEEE. https://doi.org/10.1109/OCEANS.2016.7761128
- Hollinger GA, Singh S. 2012. Multirobot coordination with periodic connectivity: theory and experiments. IEEE Trans. Robot. 28:967–73
- Ghaffarkhah A, Mostofi Y. 2012. Path planning for networked robotic surveillance. IEEE Trans. Signal Process. 60:3560–75
- Stachura M, Frew EW. 2011. Cooperative target localization with a communication-aware unmanned aircraft system. AIAA 7. Guid. Control Dyn. 34:1352–62
- Bethke B, How J, Vian J. 2009. Multi-UAV persistent surveillance with communication constraints and health management. In *Proceedings of the AIAA Guidance, Navigation, and Control Conference*, pap. 2009– 5654. Reston, VA: Am. Inst. Aeronaut. Astronaut.
- Beard RW, McLain TW. 2003. Multiple UAV cooperative search under collision avoidance and limited range communication constraints. In 42nd IEEE International Conference on Decision and Control, Vol. 1, pp. 25–30. Piscataway, NJ: IEEE
- Ghaffarkhah A, Mostofi Y. 2011. Communication-aware motion planning in mobile networks. IEEE Trans. Autom. Control 56:2478–85
- Zavlanos MM, Egerstedt MB, Pappas GJ. 2011. Graph-theoretic connectivity control of mobile robot networks. Proc. IEEE 99:1525–40
- Zavlanos MM, Pappas GJ. 2008. Distributed connectivity control of mobile networks. IEEE Trans. Robot. 24:1416–28

- Esposito JM, Dunbar TW. 2006. Maintaining wireless connectivity constraints for swarms in the presence of obstacles. In *Proceedings of the 2006 IEEE International Conference on Robotics and Automation*, pp. 946–51. Piscataway. NI: IEEE
- Ren W, Beard RW. 2005. Consensus seeking in multiagent systems under dynamically changing interaction topologies. IEEE Trans. Autom. Control 50:655–61
- Goddemeier N, Behnke D, Wietfeld C. 2013. Impact of communication constraints on consensus finding in multi-agent systems. In 2013 IEEE 24th Annual International Symposium on Personal, Indoor, and Mobile Radio Communications, pp. 2464–68. Piscataway, NJ: IEEE
- Paull L, Huang G, Seto M, Leonard JJ. 2015. Communication-constrained multi-AUV cooperative SLAM. In 2015 IEEE International Conference on Robotics and Automation, pp. 509–16. Piscataway, NJ: IEEE
- Giamou M, Khosoussi K, How JP. 2018. Talk resource-efficiently to me: optimal communication planning for distributed loop closure detection. In 2018 IEEE International Conference on Robotics and Automation, pp. 3841–48. Piscataway, NJ: IEEE
- Ponda S, Redding J, Choi HL, How JP, Vavrina M, Vian J. 2010. Decentralized planning for complex missions with dynamic communication constraints. In 2010 American Control Conference, pp. 3998

 –4003. Piscataway, NJ: IEEE
- Ponda SS, Johnson LB, Kopeikin AN, Choi HL, How JP. 2012. Distributed planning strategies to ensure network connectivity for dynamic heterogeneous teams. IEEE 7. Sel. Areas Commun. 30:861–69
- Zavlanos MM, Ribeiro A, Pappas GJ. 2012. Network integrity in mobile robotic networks. IEEE Trans. Autom. Control 58:3–18
- Kantaros Y, Zavlanos MM. 2016. Global planning for multi-robot communication networks in complex environments. IEEE Trans. Robot. 32:1045–61
- Das SM, Hu YC, Lee CSG, Lu YH. 2007. Mobility-aware ad hoc routing protocols for networking mobile robot teams. 7. Commun. Netw. 9:296–311
- Dantu K, Sukhatme GS. 2009. Connectivity versus control: using directional and positional cues to stabilize routing in robot networks. In 2009 Second International Conference on Robot Communication and Coordination. Piscataway, NJ: IEEE. https://doi.org/10.4108/ICST.ROBOCOMM2009.5846
- Lindhé M, Johansson K. 2009. Using robot mobility to exploit multipath fading. IEEE Wireless Commun. 16:30–37
- Zeng Y, Zhang R. 2017. Energy-efficient UAV communication with trajectory optimization. IEEE Trans. Wireless Commun. 16:3747–60
- Muralidharan A, Mostofi Y. 2020. Statistics of the distance traveled until successful connectivity for unmanned vehicles. Auton. Robots 44:25–42
- Jiang F, Swindlehurst AL. 2012. Optimization of UAV heading for the ground-to-air uplink. IEEE J. Sel. Areas Commun. 30:993–1005
- Muralidharan A, Mostofi Y. 2017. Path planning for a connectivity seeking robot. In 2017 IEEE Globecom Workshops. Piscataway, NJ: IEEE. https://doi.org/10.1109/GLOCOMW.2017.8269061
- Muralidharan A, Mostofi Y. 2019. Path planning for minimizing the expected cost until success. IEEE Trans. Robot. 35:466–81
- Muralidharan A, Mostofi Y. 2017. First passage distance to connectivity for mobile robots. In 2017 American Control Conference, pp. 1517–23. Piscataway, NJ: IEEE
- Stump E, Jadbabaie A, Kumar V. 2008. Connectivity management in mobile robot teams. In 2008 IEEE International Conference on Robotics and Automation, pp. 1525–30. Piscataway, NJ: IEEE
- Dixon C, Frew E. 2012. Optimizing cascaded chains of unmanned aircraft acting as communication relays. IEEE 7. Sel. Areas Commun. 30:883–98
- Yan Y, Mostofi Y. 2012. Robotic router formation in realistic communication environments. IEEE Trans. Robot. 28:810–27
- Chatzipanagiotis N, Zavlanos MM. 2016. Distributed scheduling of network connectivity using mobile access point robots. IEEE Trans. Robot. 32:1333–46
- Zeng Y, Zhang R, Lim TJ. 2016. Throughput maximization for UAV-enabled mobile relaying systems. IEEE Trans. Commun. 64:4983–96

- Fink J, Ribeiro A, Kumar V. 2013. Robust control of mobility and communications in autonomous robot teams. IEEE Access 1:290–309
- Kim Y, Mesbahi M. 2005. On maximizing the second smallest eigenvalue of a state-dependent graph Laplacian. In 2005 American Control Conference, pp. 99–103. Piscataway, NJ: IEEE
- Zhan P, Yu K, Swindlehurst AL. 2011. Wireless relay communications with unmanned aerial vehicles: performance and optimization. IEEE Trans. Aerospace Electron. Syst. 47:2068–85
- Schouwenaars T, Stubbs A, Paduano J, Feron E. 2006. Multivehicle path planning for non-line of sight communication. 7. Field Robot. 23:269–90
- Chatzipanagiotis N, Liu Y, Petropulu A, Zavlanos M. 2012. Controlling groups of mobile beamformers. In 2012 51st IEEE Conference on Decision and Control, pp. 1984

 –89. Piscataway, NJ: IEEE
- Kalogerias DS, Petropulu AP. 2016. Mobile beamforming and spatially controlled relay communications. In 2016 IEEE International Conference on Acoustics, Speech and Signal Processing, pp. 6405–9. Piscataway, NJ: IEEE
- Kalogerias DS, Petropulu AP. 2018. Spatially controlled relay beamforming. IEEE Trans. Signal Process. 66:6418–33
- Muralidharan A, Mostofi Y. 2017. Energy optimal distributed beamforming using unmanned vehicles. IEEE Trans. Control Netw. Syst. 5:1529–40
- Muralidharan A, Mostofi Y. 2016. Distributed beamforming using mobile robots. In 2016 IEEE International Conference on Acoustics, Speech and Signal Processing, pp. 6385–89. Piscataway, NJ: IEEE
- Yan Y, Mostofi Y. 2016. Efficient clustering and path planning strategies for robotic data collection using space-filling curves. IEEE Trans. Control Netw. Syst. 4:838–49
- Tekdas O, Isler V, Lim JH, Terzis A. 2009. Using mobile robots to harvest data from sensor fields. IEEE Wireless Commun. 16:22–28
- Hollinger G, Choudhary S, Qarabaqi P, Murphy C, Mitra U, et al. 2012. Underwater data collection using robotic sensor networks. IEEE 7. Sel. Areas Commun. 30:899–911
- Yan Y, Mostofi Y. 2014. To go or not to go: on energy-aware and communication-aware robotic operation. IEEE Trans. Control Netw. Syst. 1:218–31
- Carfang AJ, Frew EW, Kingston DB. 2014. Cascaded optimization of aircraft trajectories for persistent data ferrying. AIAA J. Aerosp. Inf. Syst. 11:807–20
- Say S, Inata H, Liu J, Shimamoto S. 2016. Priority-based data gathering framework in UAV-assisted wireless sensor networks. IEEE Sens. 7. 16:5785–94
- 53. Sugihara R, Gupta RK. 2011. Path planning of data mules in sensor networks. ACM Trans. Sens. Netw. 8:1
- Bhadauria D, Tekdas O, Isler V. 2011. Robotic data mules for collecting data over sparse sensor fields. 7. Field Robot. 28:388–404
- Mozaffari M, Saad W, Bennis M, Debbah M. 2017. Wireless communication using unmanned aerial vehicles (UAVs): optimal transport theory for hover time optimization. *IEEE Trans. Wireless Commun.* 16:8052–66
- Alzenad M, El-Keyi A, Yanikomeroglu H. 2017. 3-D placement of an unmanned aerial vehicle base station for maximum coverage of users with different QoS requirements. IEEE Wireless Commun. Lett. 7:38–41
- Malmirchegini M, Mostofi Y. 2012. On the spatial predictability of communication channels. *IEEE Trans. Wireless Commun.* 11:964–78
- Ghaffarkhah A, Mostofi Y. 2010. Channel learning and communication-aware motion planning in mobile networks. In 2010 American Control Conference, pp. 5413–20. Piscataway, NJ: IEEE
- Caccamo S, Parasuraman R, Freda L, Gianni M, Ögren P. 2017. RCAMP: a resilient communicationaware motion planner for mobile robots with autonomous repair of wireless connectivity. In 2017 IEEE/RS7 International Conference on Intelligent Robots and Systems, pp. 2010–17. Piscataway, NJ: IEEE
- Carfang AJ, Wagle N, Frew EW. 2015. Integrating nonparametric learning with path planning for dataferry communications. J. Aerosp. Inf. Syst. 12:784

 –99
- Kalogerias DS, Petropulu AP. 2015. Nonlinear spatiotemporal channel gain map tracking in mobile cooperative networks. In 2015 IEEE 16th International Workshop on Signal Processing Advances in Wireless Communications, pp. 660–64. Piscataway, NJ: IEEE

- Parasuraman R, Oegren P, Min BC. 2018. Kalman filter based spatial prediction of wireless connectivity for autonomous robots and connected vehicles. In 2018 IEEE 88th Vehicular Technology Conference. Piscataway. NI: IEEE. https://doi.org/10.1109/VTCFall.2018.8690611
- Narayanan VK, Miyashita T, Horikawa Y, Hagita N. 2018. A transient-goal driven communication-aware navigation strategy for large human-populated environments. In 2018 IEEE/RSJ International Conference on Intelligent Robots and Systems. Piscataway, NJ: IEEE. https://doi.org/10.1109/IROS.2018.8593827
- Nurellari E, Licea DB, Ghogho M. 2019. Optimum trajectory planning for robotic data ferries in delay tolerant wireless sensor networks. In 2019 27th European Signal Processing Conference. Piscataway, NJ: IEEE. https://doi.org/10.23919/EUSIPCO.2019.8902955
- Yan Y, Mostofi Y. 2013. Co-optimization of communication and motion planning of a robotic operation under resource constraints and in fading environments. *IEEE Trans. Wireless Commun.* 12:1562–72
- Ali U, Cai H, Mostofi Y, Wardi Y. 2018. Motion-communication co-optimization with cooperative load transfer in mobile robotics: an optimal control perspective. IEEE Trans. Control Netw. Syst. 6:621–32
- Cai H, Mostofi Y. 2019. Human-robot collaborative site inspection under resource constraints. IEEE Trans. Robot. 35:200–15
- Rappaport TS. 1996. Wireless Communications: Principles and Practice. Upper Saddle River, NJ: Prentice Hall
- Hashemi H. 1994. A study of temporal and spatial variations of the indoor radio propagation channel. In 5th IEEE International Symposium on Personal, Indoor and Mobile Radio Communications, pp. 127–34. Piscataway, NI: IEEE
- 70. Siegert AJ. 1951. On the first passage time probability problem. Phys. Rev. 81:617–23
- 71. Dudley RM. 2002. Real Analysis and Probability. Cambridge, UK: Cambridge Univ. Press
- 72. Papoulis A, Pillai SU. 2002. Probability, Random Variables, and Stochastic Processes. Boston: McGraw-Hill
- 73. Mehr C, McFadden J. 1965. Certain properties of Gaussian processes and their first-passage times. *J. R. Stat. Soc. B* 27:505–22
- Ricciardi LM, Sato S. 1988. First-passage-time density and moments of the Ornstein-Uhlenbeck process.
 Appl. Probab. 25:43–57
- Di Nardo E, Nobile A, Pirozzi E, Ricciardi L. 2001. A computational approach to first-passage-time problems for Gauss-Markov processes. Adv. Appl. Probab. 33:453–82
- 76. Cover TM, Thomas JA. 2012. Elements of Information Theory. New York: Wiley & Sons
- 77. Robert CP. 1996. Intrinsic losses. Theory Decis. 40:191–214
- Smith W, Cox D. 2004. Urban propagation modeling for wireless systems. Tech. Rep., Def. Tech. Inf. Cent., Fort Belvoir. VA
- 79. Fudenberg D, Tirole J. 1991. Game Theory. Cambridge, MA: MIT Press
- 80. Monderer D, Shapley L. 1996. Potential games. Games Econ. Behav. 14:124-43
- Marden JR, Shamma JS. 2012. Revisiting log-linear learning: asynchrony, completeness and payoff-based implementation. *Games Econ. Behav.* 75:788–808
- Tse D, Viswanath P. 2005. Fundamentals of Wireless Communication. Cambridge, UK: Cambridge Univ. Press
- Mudumbai R, Brown D III, Madhow U, Poor H. 2009. Distributed transmit beamforming: challenges and recent progress. *IEEE Commun. Mag.* 47(2):102–10
- Ochiai H, Mitran P, Poor H, Tarokh V. 2005. Collaborative beamforming for distributed wireless ad hoc sensor networks. IEEE Trans. Signal Process. 53:4110–24
- Karanam CR, Korany B, Mostofi Y. 2018. Magnitude-based angle-of-arrival estimation, localization, and target tracking. In 2018 17th ACM/IEEE International Conference on Information Processing in Sensor Networks, pp. 254

 –65. Piscataway, NJ: IEEE
- De Gennaro MC, Jadbabaie A. 2006. Decentralized control of connectivity for multi-agent systems. In 45th IEEE Conference on Decision and Control, pp. 3628–33. Piscataway, NJ: IEEE
- Dai R, Maximoff J, Mesbahi M. 2013. Optimal trajectory generation for establishing connectivity in proximity networks. IEEE Trans. Aerosp. Electron. Syst. 49:1968–81



Annual Review of Control, Robotics, and Autonomous Systems

Volume 4, 2021

Contents

| What Is Robotics? Why Do We Need It and How Can We Get It? Daniel E. Koditschek | . 1 |
|---|-----|
| The Role of Physics-Based Simulators in Robotics C. Karen Liu and Dan Negrut | 35 |
| Koopman Operators for Estimation and Control of Dynamical Systems Samuel E. Otto and Clarence W. Rowley | 59 |
| Optimal Transport in Systems and Control Yongxin Chen, Tryphon T. Georgiou, and Michele Pavon | 39 |
| Communication-Aware Robotics: Exploiting Motion for Communication Arjun Muralidharan and Yasamin Mostofi | 15 |
| Factor Graphs: Exploiting Structure in Robotics Frank Dellaert | 11 |
| Brain–Machine Interfaces: Closed-Loop Control in an Adaptive System Ethan Sorrell, Michael E. Rule, and Timothy O'Leary | 57 |
| Noninvasive Brain–Machine Interfaces for Robotic Devices Luca Tonin and José del R. Millán | 91 |
| Advances in Inference and Representation for Simultaneous Localization and Mapping David M. Rosen, Kevin J. Doherty, Antonio Terán Espinoza, and John J. Leonard | 15 |
| Markov Chain—Based Stochastic Strategies for Robotic Surveillance Xiaoming Duan and Francesco Bullo | 13 |
| Integrated Task and Motion Planning Caelan Reed Garrett, Rohan Chitnis, Rachel Holladay, Beomjoon Kim, Tom Silver, Leslie Pack Kaelbling, and Tomás Lozano-Pérez | 55 |
| Asymptotically Optimal Sampling-Based Motion Planning Methods Jonathan D. Gammell and Marlin P. Strub | 95 |

| Scalable Control of Positive Systems Anders Rantzer and Maria Elena Valcher | 319 |
|---|-----|
| Optimal Quantum Control Theory M.R. James | 343 |
| Set Propagation Techniques for Reachability Analysis Matthias Althoff, Goran Frehse, and Antoine Girard | 369 |
| Control and Optimization of Air Traffic Networks Karthik Gopalakrishnan and Hamsa Balakrishnan | 397 |
| Model Reduction Methods for Complex Network Systems X. Cheng and J.M.A. Scherpen | 425 |
| Analysis and Interventions in Large Network Games Francesca Parise and Asuman Ozdaglar | 455 |
| Animal-in-the-Loop: Using Interactive Robotic Conspecifics to Study Social Behavior in Animal Groups Tim Landgraf, Gregor H.W. Gebhardt, David Bierbach, Pawel Romanczuk, Lea Musiolek, Verena V. Hafner, and Jens Krause | 487 |
| Motion Control in Magnetic Microrobotics: From Individual and Multiple Robots to Swarms Lidong Yang and Li Zhang | 509 |
| Dynamic Walking: Toward Agile and Efficient Bipedal Robots Jenna Reher and Aaron D. Ames | 535 |
| Mechanisms for Robotic Grasping and Manipulation Vincent Babin and Clément Gosselin | 573 |
| Current Solutions and Future Trends for Robotic Prosthetic Hands Vincent Mendez, Francesco Iberite, Solaiman Shokur, and Silvestro Micera | 595 |
| Electronic Skins for Healthcare Monitoring and Smart Prostheses Haotian Chen, Laurent Dejace, and Stéphanie P. Lacour | 629 |
| Autonomy in Surgical Robotics Aleks Attanasio, Bruno Scaglioni, Elena De Momi, Paolo Fiorini, and Pietro Valdastri | 651 |
| The Use of Robots to Respond to Nuclear Accidents: Applying the Lessons of the Past to the Fukushima Daiichi Nuclear Power Station <i>Yasuyoshi Yokokohji</i> | 681 |

Errata

An online log of corrections to *Annual Review of Control, Robotics, and Autonomous Systems* articles may be found at http://www.annualreviews.org/errata/control